

See discussions, stats, and author profiles for this publication at: <https://www.researchgate.net/publication/231646426>

Kinetic Study of the Graphite Oxide Reduction: Combined Structural and Gravimetric Experiments under Isothermal and Nonisothermal Conditions

ARTICLE *in* THE JOURNAL OF PHYSICAL CHEMISTRY C · NOVEMBER 2010

Impact Factor: 4.77 · DOI: 10.1021/jp108905j

CITATIONS

25

READS

48

3 AUTHORS, INCLUDING:



Fabienne Barroso-Bujans

Center of Materials Physics

43 PUBLICATIONS 713 CITATIONS

[SEE PROFILE](#)



Juan Colmenero

Universidad del País Vasco / Euskal Herrik...

401 PUBLICATIONS 8,419 CITATIONS

[SEE PROFILE](#)

Kinetic Study of the Graphite Oxide Reduction: Combined Structural and Gravimetric Experiments under Isothermal and Nonisothermal Conditions

Fabienne Barroso-Bujans,^{*,†} Ángel Alegria,^{†,‡} and Juan Colmenero^{†,‡,§}

Material Physics Center (CSIC-UPV/EHU), Paseo Manuel de Lardizábal 5, 20018 San Sebastián, Spain, Departamento de Física de Materiales, Universidad del País Vasco (UPV/EHU) Apartado 1072, 20080 San Sebastián, Spain, and Donostia International Physics Center, Paseo Manuel de Lardizábal 4, 20018 San Sebastián, Spain

Received: September 17, 2010; Revised Manuscript Received: November 5, 2010

The mechanisms involved in the thermal reduction of graphite oxide (GO) are not yet clear. In the present study, the thermal reduction of GO, obtained by a Brodie-based method, is monitored by means of time- and temperature-resolved X-ray diffraction (XRD), thermogravimetric analysis (TGA), and TGA/mass spectrometry (MS) in dynamic (nonisothermal) and static (isothermal) modes. Two distinct mechanisms were well resolved by the fitting of isothermal TGA data to 2D diffusion and autocatalytic models, which provides new insights on the thermal behavior of GO. The combined TGA and XRD results in isothermal mode suggest that the 2D diffusion mechanism mainly occurs in the interlayer, whereas the autocatalytic mechanism occurs in the external surface. The latter overcomes the former when GO has lost about 10 wt %. The results are compared to previous studies on the thermal reduction of GO. The differences found could be attributed to the synthetic method used to obtain GO.

1. Introduction

Graphite oxide (GO) has been known since the 19th century but it has recently re-emerged as an intensive research area due to its importance in obtaining large-scale graphene materials,^{1,2} afforded by the chemical^{3–5} or thermal reduction^{6,7} of GO, among others.⁸ Chemical reduction involves the use of reducing agents such as hydrazine,³ hydroquinone,⁴ and NaBH₄,⁵ whereas the thermal treatment^{6,7} at elevated temperatures avoids the use of these hazardous chemicals and provides a rapid and efficient method to produce large amounts of graphenelike sheets.

GO is an oxygen-rich derivative of graphite, where the carbon layers lose their planarity to become corrugated due to the conversion of many of the sp² carbon atoms into sp³ ones. One of the most accepted models is that proposed by Lerf et al.,^{9,10} recently supported by Casabianca et al.¹¹ using a combination of multidimensional ¹³C solid-state NMR techniques and ab initio chemical shift calculations. This model established the existence of 1,2 epoxide and hydroxyl groups on the GO basal planes, whereas ketonic and carboxylic groups are localized at the edge of GO sheets.

Oxygen functional groups of GO decompose exothermically upon heating, thus evolving a gas mainly composed of H₂O, CO, and CO₂.^{6,7,12} When the gas pressure exceeds the van der Waals forces that hold the GO layers, exfoliation takes place.⁷ The transformation of functional groups of GO upon chemical^{3–5} or thermal reduction^{6,7} has been systematically studied in the past by means of ¹³C NMR,¹³ XPS,^{13–16} elemental analysis,¹⁷ Raman,^{14,15,18} and FTIR spectroscopy,^{17,19} electrical,^{12,15} and optical measurements,¹⁵ atomic force microscopy,¹⁶ XRD,¹⁷ and so forth. The restoration of C=C bonds and a decrease in the number of C–OH, C–O–C, COOH groups have been ob-

served. However, deoxygenation is not complete and different residual amounts of oxygen were detected in the final product depending on the reduction process (temperature, atmosphere, treatment). Studies by molecular dynamics simulations showed that the oxygen amount remaining in reduced GO was also dependent upon the initial oxygen concentration and the hydroxyl/epoxide ratio.¹⁹ Because a great variety of GOs can be obtained (the most well-known synthesis methods are those of Brodie,²⁰ Hummers,²¹ and Staudenmaier²²) the composition and, therefore, the chemical-physical properties of reduced GO, can be extensively different. As an example, the electrical resistivity and surface areas measured by Steurer et al.²³ were higher in the thermally reduced GO prepared by the Brodie method than in that obtained by the Hummers method.

The mechanisms involved in the thermal reduction of GO are far from clear and no predictions can be made on the final properties of the reduced GO. For that reason, intensive studies on the thermal reduction of GO are of great importance, especially when combining different experimental techniques to provide structural and compositional information. Following this idea, in the present study, temperature- and time-resolved XRD and TGA are used to monitor the structural changes of GO, prepared by a Brodie-based method, upon dynamic (nonisothermal) and static (isothermal) modes. Simultaneous TGA/MS experiments are also conducted in both modes to gain insight in the reduction reactions taking place. Isothermal TGA is run at various temperatures in the 160–200 °C range, allowing the establishment of the kinetic mechanisms involved in the thermal reduction of GO.

2. Experimental Section

Graphite oxide was produced from natural graphite from Alfa Aesar, reference 40799, universal grade, 200-mesh, 99.9995% (metal basis). The graphite was oxidized using a Brodie-based method.^{20,24} Briefly, a reaction flask containing 200 mL fuming nitric acid (Fluka) was cooled to 0 °C with a cryostat bath for

* To whom correspondence is addressed. Fax: +34 943 212236. E-mail: fbarroso@ehu.es.

† Material Physics Center (CSIC-UPV/EHU).

‡ Universidad del País Vasco (UPV/EHU).

§ Donostia International Physics Center.

20 min and then 10 g of graphite were introduced. Next, 80 g of potassium chlorate (Fluka) was slowly added over 1 h, to avoid sudden increases in temperature, and the reaction mixture was stirred for 21 h at 0 °C. The mixture was diluted in distilled water and filtered until the supernatant had a nitrate content lower than 1 mg/L (AQUANAL-plus nitrate (NO_3) 1–50 mg/L). The GO slurry was dried at 80 °C for 24 h in a vacuum oven ($P < 0.1$ mbar) and stored in this oven at room temperature until use. Elemental analysis of the so obtained GO showed an atomic composition of $\text{C}_{8}\text{H}_{1.3}\text{O}_{2.6}$. Additional compositional information can be found in ref 27.

Temperature-resolved XRD data in dynamic mode were collected upon heating at 1 °C/min from room temperature to 600 °C on a Bruker D8 Advance diffractometer operating at 30 kV and 20 mA, equipped with a Cu tube ($\lambda = 1.5418$ Å), a Vantec-1 PSD detector, and an Anton Parr HTK2000 high-temperature furnace. An isothermal experiment was run in a PHILIPS X'PERT PRO automatic diffractometer operating at 40 kV and 40 mA, in theta-theta configuration by heating first at 10 °C/min from room temperature to 100 °C, followed by a ramp at 1 °C/min to the desired temperature (200 °C). During the isothermal data collection, for 14 h the sample temperature remained constant within 0.5 K. A secondary monochromator with Cu radiation ($\lambda = 1.5418$ Å), a PIXcel solid-state detector and a high-temperature furnace (Anton Parr HTK16) were used in this later experiment.

Thermogravimetry in dynamic and isothermal modes was carried out in a TGA Q500 from TA Instruments, by using a constant N_2 flow of 60 mL/min. The same temperature programs as those in the XRD experiments were used. For the kinetic study, isothermals were registered at five temperatures in the 160–200 °C range. Reliability of sample temperatures was carefully checked from the derivative thermogravimetric (DTG) peak corresponding to the Curie temperature of nickel.

TGA/MS was carried out using another TGA Q500, different from the previous one, coupled to a Pfeiffer Vacuum ThermoStar™ mass spectrometer equipped with a channeltron detector. These isothermal and dynamic experiments were recorded under constant He flow of 90 mL/min. Isotherm TGA/MS was registered at 220 °C for about 8 h and the dynamic TGA/MS at 1 °C/min. The evolved gas was ionized and its components detected according to the mass to charge (m/z) ratio.

The morphology of the natural graphite used and its relative GO and thermally reduced GO (Tr-GO) was studied by scanning electron microscopy (SEM). This step was performed with a TM3000 Tabletop microscope from Hitachi. Tr-GO samples were prepared by slow and fast heating rates. The sample obtained in the TGA after running a dynamic experiment at 1 °C/min up to 800 °C in N_2 stream and subsequent cooling down to room temperature was named Tr-GO (slow). A second Tr-GO obtained by a fast heating rate Tr-GO (fast) was obtained by placing the GO in a glass boat and inserting it in a quartz tube under an argon flux. This tube was inserted in a tube furnace preheated to 1000 °C and kept for 1 min. Then, the sample was kept within the quartz tube until reaching room temperature.

3. Results and Discussion

3.1. Dynamic Experiments. Figure 1 shows the GO XRD profiles obtained in a dynamic heating program up to 600 °C. In the temperature interval where exfoliation is expected to occur (between 200 and 265 °C), a progressive reduction of intensity of the 001 reflection peak ($2\theta \approx 16^\circ$) was observed. With increasing temperature, a peak at $2\theta \approx 20^\circ$ developed in an

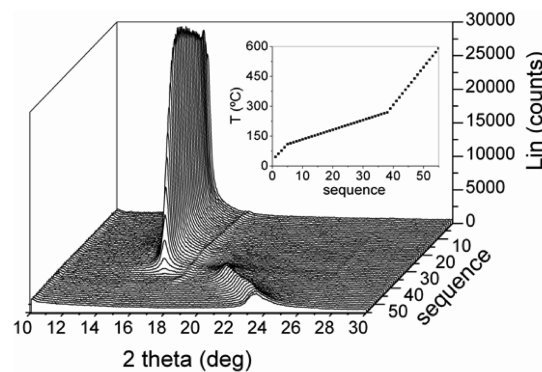


Figure 1. Temperature-resolved XRD profiles of GO. Insert: Correspondence of temperature with sequence of the 3D graph.

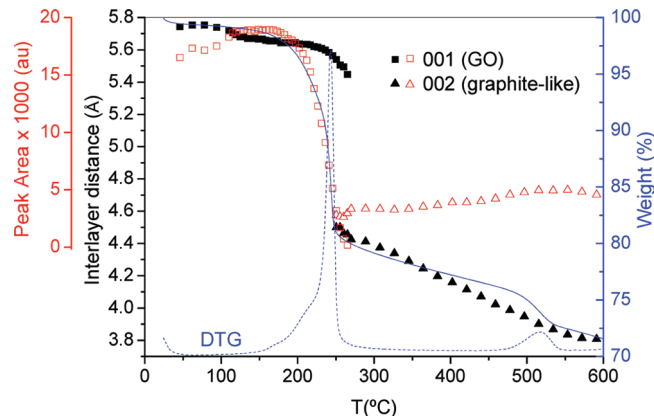


Figure 2. Overlapping of TGA and DTG profiles with the variation of the interlayer distance and peak area obtained by means of temperature-dependent XRD. Blue solid line: TGA profile. Blue dashed line: DTG profile. Black filled figures: interlayer distance associated with GO (square) and graphitelike structures (triangle). Red open symbols: peak area of the corresponding GO and graphitelike structure reflections.

intermediate position between that of GO and native graphite ($2\theta = 26.6^\circ$), indicating the partial restacking of the reduced GO layers.⁷ This signal was then assigned as the 002 reflection of graphitelike structures.

The variation of the interlayer distance, calculated from the Bragg diffraction angle of the 001 and 002 peaks, and the variation of the integrated peak areas, were compared with that of the weight loss obtained from TGA in an independent experiment (Figure 2). From room temperature to about 130 °C, before GO reduction, the loss of absorbed moisture occurred but with insignificant changes in the GO weight (special care was taken by rapidly moving the sample from the vacuum oven to the TGA equipment). However, this small water loss at 100 °C affected both the 001 peak area, which showed a marked increase, and the interlayer distance, which decreased only 0.1 Å. Because the peak area intensities are a true measure of the amount of stacking layer present, the results suggest that water deintercalation allows the GO layers to both closely approach and stack.²⁵ This idea is also supported by our previous time-resolved XRD studies on water desorption from GO.^{24,26}

GO reduction started at about 150 °C and seemed to occur in two partially overlapped processes (see a shoulder before the sharp peak in the DTG curve). In this temperature range, the TGA curve showed 20 wt % weight loss and the 001 peak area showed a dramatic reduction down to the detection limit. The close overlapping of both mass loss and 001 peak area decrease indicates that deoxygenation of GO leads to a complete loss of

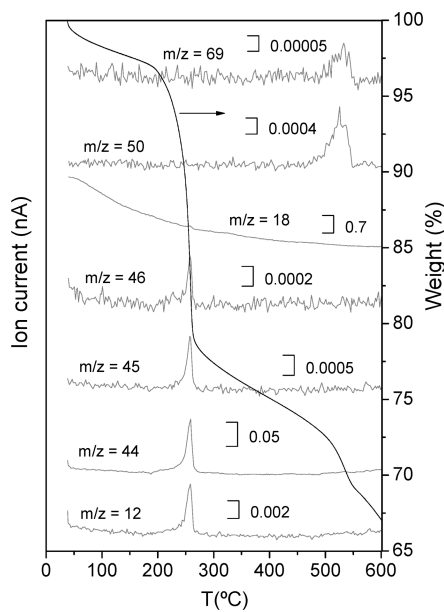


Figure 3. Dynamic TGA/MS of GO at 1 °C/min in helium stream.

any stacked-layer structure in GO. However, it seems that the onset of GO reduction does not produce any significant structure loss (observe that the 001 peak area is slightly delayed with respect to the weight loss), suggesting that either the pressure generated by the released gas is still below the van der Waals forces that hold together the GO layers and/or the lateral diffusion can relieve the pressure.⁷ Furthermore, the interlayer distance of GO started to collapse at 220 °C, where a second process prevailed over the starting one (DTG curve). In this process, the main reduction mechanism occurs. Most of the GO layers exfoliate (decreasing peak area) but others seem to move closer together (decreasing interlayer distance) due to the release of the oxygen-functional groups. At the end of this process, the 001 peak disappeared and the 002 reflection from graphitelike structures⁷ emerged. The 002 peak area then increased to a maximum value at 500 °C, accompanied by a regular decrease in both weight and interlayer distance. These data are consistent with the re-emergence of graphitic order in the Tr-GO, which is also supported by Raman spectroscopy data.^{14,15,18} With increasing temperature, partial recovery of planar sp^2 carbon structure allows the formation of stacked layer zones with an interlayer spacing very close to that of native graphite. The broad shape of the 002 peak (Figure 1) accounts for the still corrugated structure of Tr-GO sheets.⁷ A third process was observed to start at 460 °C with 3.5 wt % of weight loss, which did not appreciably affect the interlayer distance and the 002 peak area.

The simultaneous TGA/MS allowed the compositional analysis of the evolved gas (Figure 3). The detected peaks with $m/z = 12, 43$ (not shown), 44, 45, and 46 showed maximum ion currents at 220 °C, whereas those with $m/z = 50$ and 69 showed a maximum at 490 °C. However, the signal with $m/z = 18$, attributed to H_2O^+ , showed a decreasing curve, where a small peak was detected at 220 °C. Ions with $m/z = 12 (C^+)$ and 44 (CO_2^+) are attributed to CO_2 . Ions with $m/z = 45$ and 46 would likely arise from isotopes of CO_2^+ ions [$m/z = 45 (^{13}CO_2^+)$ and $m/z = 46 (^{18}CO_2^+)$]. This signal assignment is based on the fact that the relative signal intensities of peaks 45/44 (1.3%) and 46/44 (0.6%) reflect the relative abundance of ^{13}C (1.1%) and ^{18}O (0.2%), respectively.²⁷ The low-intensity signal with $m/z = 43$ could arise from $C_2H_3O^+$ fragments. The high-temperature peaks with $m/z = 50$ and 69 indicate that larger molecules, which come from stable structures in a relatively low amount (3.5 wt %), were released. The assignment of these signals is rather complicated due to the heterogeneity of groups in GO.

3.2. Isothermal Experiments. To get more detailed information about the GO reduction process that occurs at about 200 °C, new XRD, TGA, and TGA/MS experiments were run but in isothermal mode. The advantage of the isothermal methods over the dynamic ones is that the reaction time can be long and in this situation the reaction rate is likely to be controlled by reaction kinetics rather than by heat transfer. Figure 4 shows the XRD profiles obtained during an isothermal program. The experiment was performed through a rapid increase of the temperature from room temperature to 100 at 10 °C/min, followed by a slow increase at 1 °C/min (to avoid possible deflagration) to 200 °C, at which the isotherm was run (insert of Figure 4). The 001 peak intensity decreased over the isothermal region and the 002 reflection of graphitelike structures emerged during the longest times. However, in contrast to the dynamic experiment, the 001 reflection did not disappear completely at comparable weight loss (80 wt %, TGA, Figure 5). It is likely that in the static experiment the evolved-gas pressure was relatively lower than in the dynamic heating, thus causing less layer distortions and less exfoliation.

Figure 5 combines the results obtained by XRD and TGA. The TGA profile clearly showed two steps (I and II) in the isothermal range, thus, the two processes previously observed in the dynamic TGA at about 200 °C, can be readily resolved in this experiment. These results suggest that the GO reduction proceeded by two distinct kinetic mechanisms. The decay of both peak area and the interlayer distance also showed two regimes. The first regime showed a steeper decay for both peak area and interlayer distance, whereas the second one depicted a

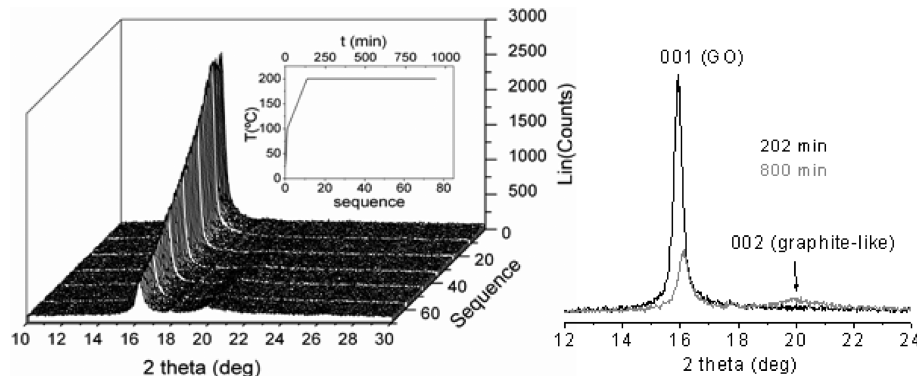


Figure 4. Left: Time-resolved XRD isothermal profiles of GO. Insert: Time–temperature-sequence correlation. Right: Comparison between diffractograms registered at 202 and 800 min.

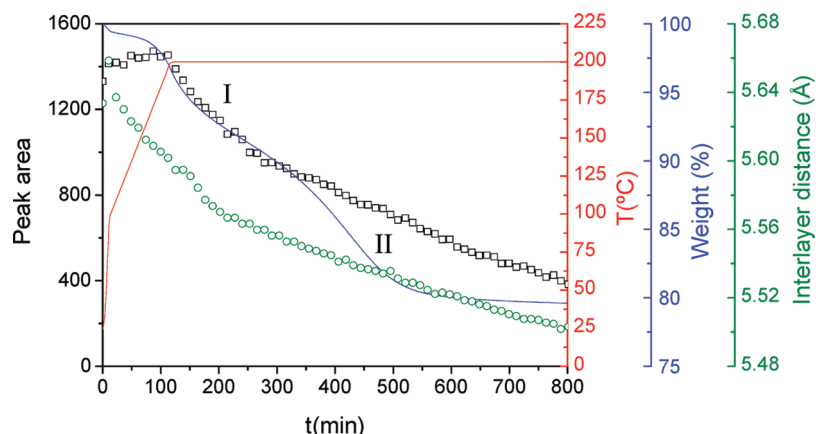


Figure 5. Isothermal reduction of GO at 195 °C. Black squares: variation of the peak area at $2\theta \approx 16^\circ$. Red line: temperature program. Blue line: weight loss (data obtained in TGA under N₂ flow). Green circles: interlayer distance.

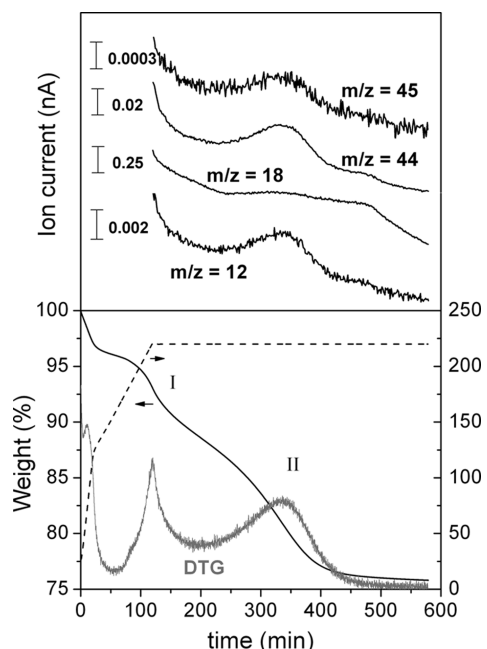


Figure 6. Isothermal reduction of GO by TGA/MS ($T = 220$ °C, gas: Helium). Bottom: TGA and DTG profiles obtained by using the temperature program plotted with dashed line. Top: MS for ions with $m/z = 12$ (C⁺), 18 (H₂O⁺), 44 (CO₂⁺), and 45 (¹³CO₂⁺).

rather regular decrease. After 550 min, the peak area and interlayer distance continued decreasing without showing a substantial mass loss.

To gain further insight on the two distinct reduction mechanisms of GO, evolved gas analysis was simultaneously performed by using isothermal TGA/MS (Figure 6). This experiment was run in a helium, instead of nitrogen, atmosphere, showing similar reduction behavior but with a slightly slower rate (the isotherm was run at 220 °C to reach similar reduction times to that run at 200 °C in N₂). In the isothermal region, the evolved gas was detected to be composed of CO₂ [$m/z = 12$ (C⁺), 44 (CO₂⁺), 45 (¹³CO₂⁺)] and H₂O [$m/z = 18$ (H₂O⁺)], as observed in the dynamic reduction of GO (Figure 3). The experiment revealed a maximum amount of released gas components (except H₂O) in step II, whereas in step I the amount of all the evolved gas components decreased rather regularly. Note that except for H₂O, the rate of the detected evolved gas components mirrored the rate of weight loss. The evolution of CO₂ and H₂O seems to indicate that GO reduction continued beyond step II.

3.3. Kinetics of the Thermal Reduction. To determine the kinetic mechanism of GO reduction, the isothermal weight loss at different temperatures (under N₂ atmosphere) was analyzed in detail (part a of Figure 7). In this representation, it is very apparent that two different mechanisms for weight loss exist, each dominating a particular range. At the lowest temperatures only mechanism I is detectable after 120 h, yielding a weight loss of about 10 wt %. At 170 °C the mechanism II can already be detected and completed (producing an extra weight loss of about 12 wt %) in a very long experiment (more than 100 h). Both processes are well-resolved and present rather different characteristics. For mechanism I, the rate decreases rapidly with the transformation, namely at the earliest stages, whereas for mechanism II, a clear maximum rate is obtained at intermediate times. These results are in perfect agreement with those already seen in the nonisothermal scan. It is noteworthy that, as we will see below, none of these mechanisms agree with the second-order kinetics reported by both McAllister et al.⁷ and Jung et al.¹² The former authors described isothermal experiments with a GO prepared from the Staudenmaier method and the latter authors used temperature-dependent resistivity measurements to study the thermal reduction of a single graphene oxide sheet obtained from GO produced by a modified Hummers method. This fact is illustrated in part a of Figure 7 by a dashed line, which represents how a second-order mechanism would look as compared to our experimental findings. Neither the process as a whole nor any of the two resolved ranges follows such behavior.

Thus, the experimental curves were separately fitted in the two ranges by selecting the most adequate mathematical functions²⁹ describing different reaction types. The general reaction rate equation is: $(d\alpha)/(dt) = k(T)f(\alpha)$, where α is the degree of conversion ($\alpha(0) = 0 \leq \alpha(t) \leq \alpha(\infty) = 1$), $k(T)$ is the temperature-dependent rate constant, and $f(\alpha)$ depends on the reaction mechanism. The best fitting for mechanism I (part b of Figure 7) was accomplished with a 2D diffusion model ($f(\alpha) = -(1)/(\ln(1 - \alpha))$) whereas for mechanism II an autocatalytic model ($f(\alpha) = \alpha^M(1 - \alpha)^N$ with $N = 3/2$ and $M = 4$) was found very adequate (part c of Figure 7). The indexes M and N in this case have, however, only an empirical significance, where their values determine relative contributions from the acceleratory and decay regions.³⁰

The main parameters arising from this fitting procedure are the corresponding rate constants $k_I(T)$ and $k_{II}(T)$. It is expected that the temperature dependence of these rate constants follows the Arrhenius equation, which indeed is the case as illustrated

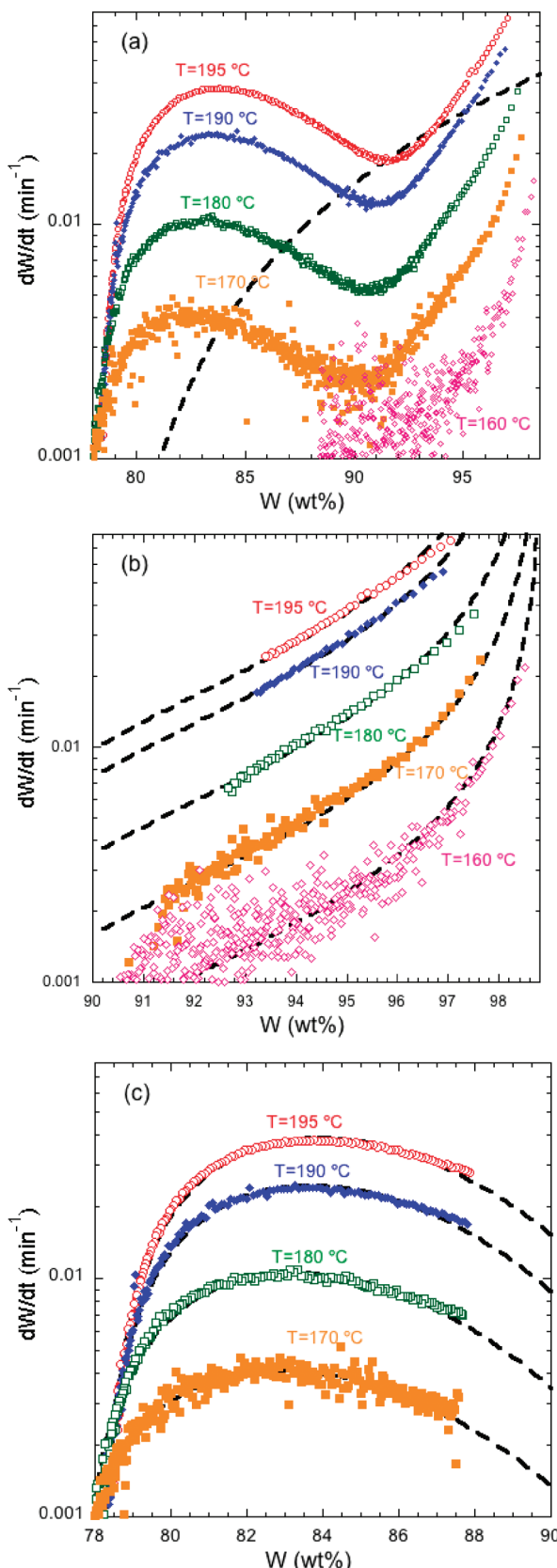


Figure 7. Rate of weight loss (dW/dt) of GO as a function of percentage weight loss (W) at different temperatures. a) Whole process, dashed line depicts a second-order mechanism; b) mechanism I, fitting curves with a 2D diffusion model, and c) mechanism II, fitting curves with an autocatalytic model.

in Figure 8, in which it is apparent that the activation energy (32.5 kcal/mol) of mechanism I is only slightly lower than that

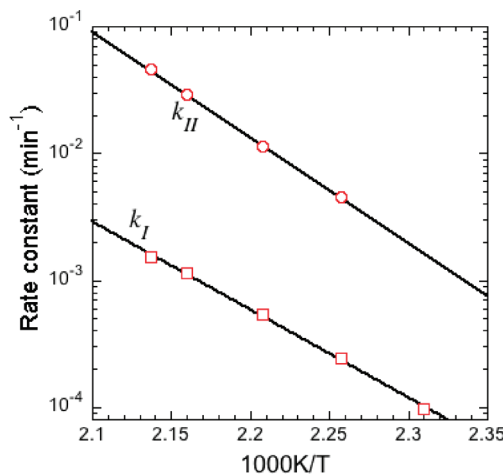


Figure 8. Arrhenius plot of the 2D diffusion (I) and autocatalytic (II) mechanisms.

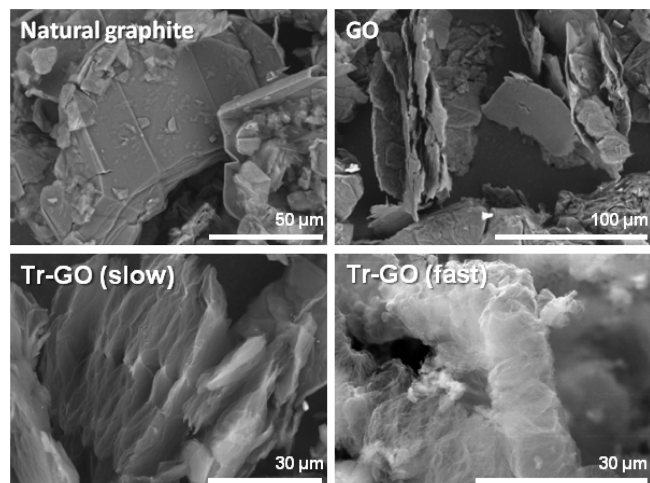


Figure 9. Representative SEM micrographs of natural graphite, GO and Tr-GO obtained by slow and fast heating rates.

of mechanism II (38.1 kcal/mol). However, the fact that the two rate constants approach each other at low temperatures does not imply that the two mechanisms become more overlapped because the experiments show that the overlapping increases slightly with temperature (part a of Figure 7). This apparently contradictory result is due to the very different natures of the two mechanisms.

The activation energy of the 2D-diffusion (mechanism I) obtained here is in very good agreement with that obtained by Jung et al.¹² by means of temperature programmed desorption measurements (TPD) of a multilayered GO film. Moreover, surprisingly, the activation energy of the autocatalytic range (mechanism II) is also similar to that found by the same authors in the reduction of a single graphene sheet, 37 kcal/mol in this case, obtained by means of resistivity measurements.

SEM micrographs of Figure 9 show the laminar structure responsible for the existing 2D-spaces in GO and Tr-GO. The planar shapes of native graphite flakes are kept after both oxidation and thermal reduction. Other transformations taking place in GO, like the size reduction of flakes, are reported elsewhere.⁷ The appearance of the accordion-like structures in Tr-GO caused by the gas diffusion at slow heating rate (1 °C/min) is remarkable. This picture is noticeably different when the gas is released under a fast heating rate. The sudden increase

of the gas pressure in the interlayer causes rapid gas diffusion in all directions, pushing the GO planes far away from their original positions. As a result, accordions produced under a fast heating rate are much more extended than those produced under a low heating rate; the volume of Tr-GO (fast) is 200 times higher than that of GO, whereas that of Tr-GO (slow) remained practically the same.

3.4. Mechanistic Models. The combination of isothermal XRD and TGA/MS experiments allowed us to confirm the presence of two well-resolved distinct reduction mechanisms of a GO prepared using a Brodie-based method. Furthermore, the comparison of structural and thermal data allowed us to identify the origin of both 2D-diffusion and autocatalytic mechanisms. The first step in the isothermal weight loss was correlated with a concomitant reduction of both the interlayer distance and the 001 peak area (Figure 5). This led us to propose that deoxygenation starts in the interlayer regions. This reaction generates ~10 wt % of a gas composed of CO₂ and H₂O, which presumably leave the interlayer space via diffusion along the GO sheets.

Although the diffusion of the evolved gas was discussed by McAllister et al.,⁷ the authors did not find experimental evidence of a diffusion mechanism in the studied temperature interval. The main difference between the two GO results is in the preparation procedure and therefore, the oxidation degree. The lower oxidation degree in our GO likely allowed us to separate both diffusion and autoacceleration processes. Note that the O/C atomic ratio of our GO (0.3) is much lower than that obtained by Schniepp and McAllister^{6,7} (0.7).

The subsequent mechanism was determined to be autocatalytic. This mechanism was not clearly related to important structural changes accompanying the weight loss (Figure 5), either in the 001 peak area or in the interlayer distance. This could be interpreted as an indication of reactions occurring outside the interlayer space. The fact that this mechanism is autoaccelerated suggests that the continuous creation of external surface promotes subsequent deoxygenation reactions. The formation of carbonyl groups via transfer reactions of hydrogen and oxygen atoms (hydrogen assisted mechanism for epoxide migration), and their subsequent breaking to produce CO, was explained as a likely mechanism of GO reduction.³¹ This mechanism, though it does not explain the experimentally observed release of CO₂ and H₂O, could partially explain the autoacceleration. CO is released from the GO sheet, leaving holes or vacancies,^{19,31} which would lead to the creation of new carbonyl and hydroxyl groups via atom migration.³¹ Thus, additional CO groups could leave the GO sheet.

Conclusions

The study of the thermal reduction of GO has revealed new experimental evidence of the kinetic mechanisms involved. Whereas combined dynamic TGA and temperature-resolved XRD allow the monitoring of the structural changes taking place in GO during the thermal reduction, isothermal methods were more effective. Combined isothermal-TGA and time-resolved XRD showed that two distinct and well-resolved mechanisms are involved in the thermal reduction of GO. Initially, 2D-diffusion takes place followed by the autocatalysis. Moreover, the combination of structural and thermal data suggested that deoxygenation starts in the interlayer and that the diffusion of the released gas causes the loss of stacking layers. When GO loses about 10 wt %, the autocatalytic process gains importance and reactions start

occurring, mainly in the external surface of GO layers (i.e., individual sheets and holes). Then, newly formed surfaces autocatalyse the evolution of further CO₂ and H₂O.

The apparent discrepancies with the previously reported second-order mechanisms by McAllister et al.⁷ and Jung et al.¹² seem to arise from the type of GO used. The GO of the present study was produced by a Brodie-based method, whereas the other GOs were obtained by the Staudenmaier⁷ and a modified Hummers methods.¹² Thus, the synthetic method and the oxidation degree of GO are likely important factors in determining the mechanisms of its reduction. However, the activation energy of this process seems not to be affected by such factors. The activation energy values obtained in both the diffusion mechanism and the autocatalysis agree well with those found by Jung et al.¹² for both multilayer and single layer graphene oxide, respectively.

Acknowledgment. The authors gratefully acknowledge the support of the Spanish Ministry of Education, project CSD2006-00053; the European Union, project 502235-2 (SOFTCOMP program) and the Basque Government, project IT-436-07. F Barroso-Bujans acknowledges a JAE-Doc contract from CSIC. We thank Dr. Aitor Larrañaga, from SGIker UPV/EHU, Leioa, for his help in performing and analyzing the XRD experiments.

References and Notes

- (1) Allen, M. J.; Tung, V. C.; Kaner, R. B. *Chem. Rev.* **2010**, *110*, 132–145.
- (2) Zhu, Y.; Murali, S.; Cai, W.; Li, X.; Suk, J. W.; Potts, J. R.; Ruoff, R. S. *Adv. Mater.* **2010**, *22*, 3906–3924.
- (3) Stankovich, S.; Dikin, D. A.; Piner, R. D.; Kohlhaas, K. A.; Kleinhammes, A.; Jia, Y.; Wu, Y.; Nguyen, S. T.; Ruoff, R. S. *Carbon* **2007**, *45*, 1558–1565.
- (4) Wang, G.; Yang, J.; Park, J.; Gou, X.; Wang, B.; Liu, H.; Yao, J. *J. Phys. Chem. C* **2008**, *112*, 8192–8195.
- (5) Shin, H.-J.; Kim, K. K.; Benayad, A.; Yoon, S.-M.; Park, H. K.; Jung, I.-S.; Jin, M. H.; Jeong, H.-K.; Kim, J. M.; Choi, J.-Y.; Lee, Y. H. *Adv. Funct. Mater.* **2009**, *19*, 1987–1992.
- (6) Schniepp, H. C.; Li, J.; McAllister, M. J.; Sai, H.; Herrera-Alonso, M.; Adamson, D. H.; Prud'homme, R. K.; Car, R.; Saville, D. A.; Aksay, I. A. *J. Phys. Chem. B* **2006**, *110*, 8535–8539.
- (7) McAllister, M. J.; Li, J.; Adamson, D. H.; Schniepp, H. C.; Abdala, A. A.; Liu, J.; Herrera-Alonso, M.; Milius, D. L.; Car, R.; Prud'homme, R. K.; Aksay, I. A. *Chem. Mater.* **2007**, *19*, 4396–4404.
- (8) Lerf, A.; He, H.; Forster, M.; Klinowski, J. *J. Phys. Chem. B* **1998**, *102*, 4477–4482.
- (9) He, H.; Riedl, T.; Lerf, A.; Klinowski, J. *J. Phys. Chem.* **1996**, *100*, 19954–19958.
- (10) Casabianca, L. B.; Shaibat, M. A.; Cai, W. W.; Park, S.; Piner, R.; Ruoff, R. S.; Ishii, Y. *J. Am. Chem. Soc.* **2010**, *132*, 5672–5676.
- (11) Zhu, Y.; Murali, S.; Stoller, M. D.; Velamakanni, A.; Piner, R. D.; Ruoff, R. S. *Carbon* **2010**, *48*, 2106–2122.
- (12) Jung, I.; Field, D. A.; Clark, N. J.; Zhu, Y.; Yang, D.; Piner, R. D.; Stankovich, S.; Dikin, D. A.; Geisler, H.; Ventrice, C. A.; Ruoff, R. S. *J. Phys. Chem. C* **2009**, *113*, 18480–18486.
- (13) Gao, W.; Alemany, L. B.; Ci, L.; Ajayan, P. M. *Nat. Chem.* **2009**, *1*, 403–408.
- (14) Yang, D.; Velamakanni, A.; Bozoklu, G.; Park, S.; Stoller, M.; Piner, R. D.; Stankovich, S.; Junga, I.; Field, D. A.; Ventrice, C. A.; Ruoff, R. S. *Carbon* **2009**, *47*, 145–152.
- (15) Mattevi, C.; Eda, G.; Agnoli, S.; Miller, S.; Mkhoyan, K. A.; Celik, O.; Mastrogiiovanni, D.; Granozzi, G.; Garfunkel, E.; Chhowalla, M. *Adv. Funct. Mater.* **2009**, *19*, 2577–2583.
- (16) Akhavan, O. *Carbon* **2010**, *48*, 509–519.
- (17) Jeong, H.-K.; Lee, Y. P.; Jin, M. H.; Kim, E. S.; Bae, J. J.; Lee, Y. H. *Chem. Phys. Lett.* **2009**, *470*, 255–258.
- (18) Kudin, K. N.; Ozbas, B.; Schniepp, H. C.; Prud'homme, R. K.; Aksay, I. A.; Car, R. *Nano Lett.* **2008**, *8*, 36–41.
- (19) Bagri, A.; Mattevi, C.; Acik, M.; Chabal, Y. J.; Chhowalla, M.; Shenoy, V. B. *Nat. Chem.* **2010**, *2*, 581–587.
- (20) Brodie, B. C. *Philos. Trans. R. Soc. London* **1859**, *149*, 249–259.
- (21) Hummers, W. S.; Offeman, R. E. *J. Am. Chem. Soc.* **1958**, *80*, 1339.
- (22) Staudenmaier, L. *Ber. Dtsch. Chem. Ges.* **1898**, *31*, 1481–1487.

- (23) Steurer, P.; Wissert, R.; Thomann, R.; Mülhaupt, R. *Macromol. Rapid Commun.* **2009**, *30*, 316–327.
- (24) Cerveny, S.; Barroso-Bujans, F.; Alegría, A.; Colmenero, J. *J. Phys. Chem. C* **2010**, *114*, 2604–2612.
- (25) Seredych, M.; Bandosz, T. *J. Langmuir* **2010**, *26*, 5491–5498.
- (26) Barroso-Bujans, F.; Cerveny, S.; Alegría, A.; Colmenero, J. *Carbon* **2010**, *48*, 3277–3286.
- (27) McLafferty, F. W.; Tureček, F. *Interpretation of Mass Spectra*; University Science Books: Sausalito, CA, 1993.
- (28) Barroso-Bujans, F.; Cerveny, S.; Verdejo, R.; del Val, J. J.; Alberdi, J. M.; Alegría, A.; Colmenero, J. *Carbon* **2010**, *48*, 1079–1087.
- (29) Málek, J.; Mitsuhashi, T.; Criado, J. M. *J. Mater. Res.* **2001**, *16*, 1862–1871.
- (30) Brown, M. E. *Thermochim. Acta* **1997**, *300*, 93–106.
- (31) Paci, J. T.; Belytschko, T.; Schatz, G. C. *J. Phys. Chem. C* **2007**, *111*, 18099–18111.

JP108905J